

Cosmic tomographies: baryon acoustic oscillations and weak lensing

Hu Zhan

Department of Physics, University of California, Davis, CA 95616, USA

E-mail: zhan@physics.ucdavis.edu

Abstract. We explore the complementarity between two tomographic probes of the universe: baryon acoustic oscillations (in the galaxy power spectrum) and weak gravitational lensing. The galaxy power spectrum characterises the density fluctuations, whereas the weak lensing shear power spectrum is a direct measure of the potential fluctuations. We find that photometric measurements of baryon oscillations alone do not provide very tight constraints on the dark energy equation of state parameters, partially due to our uncertain knowledge of the galaxy clustering bias. Weak lensing, on the other hand, is adversely impacted by the uncertainties of the probability distribution of photometric redshift errors. A *joint* analysis of the two, however, is more robust to these uncertainties and leads to a remarkable improvement over the results of either probe alone.

Forecasts of cosmological constraints with baryon oscillations and weak lensing are provided for four proposed multiband imaging surveys in combination with measurements of the cosmic microwave background from *Planck*. In particular, we find that the joint analysis of galaxy and shear power spectra with the Large Synoptic Survey Telescope can tighten the 1σ error bounds on the dark energy equation of state (at the pivot expansion factor $a_p = 0.63$) and its rate of change, respectively, to 0.016 and 0.16 (marginalized over 131 other parameters). With supernovae and cluster counting as well as higher-order statistics of the same galaxy and shear data, one can further improve the constraints.

To allow greater flexibility in utilising our forecasts, we will make our forecasting tool available publicly.

Keywords: cosmological constant experiments, gravitational lensing, power spectrum, surveys galaxies

1. Introduction

The apparent accelerated expansion of the universe revealed by type Ia supernova (SN) distances [1, 2, 3, 4] suggests the existence of an unknown component – dark energy – of the universe that drives the acceleration with its negative equation of state (EOS). Observations of the large-scale structure and cosmic microwave background (CMB) also point to the scenario that the universe is nearly flat with more than 70% of its content in dark energy [5, 6, 7, 8, 9].

Since it is not directly observable, one has to infer dark energy properties from its impact on the distance–redshift and growth–redshift relationship. Aside from SNe, baryon acoustic oscillations (BAOs) in the galaxy power spectrum and weak lensing (WL) can be used to measure the angular diameter distance. The BAO technique relies on the standard ruler of the sound horizon at the last scattering surface [10, 11, 12], which has been accurately measured by the Wilkinson

Microwave Anisotropy Probe (*WMAP*) [9] and will be further improved by future CMB experiments. WL measures the distance from its geometric lensing kernel as well as the shape of shear power spectra, and it is sensitive to the growth–redshift relationship [13, 14, 15, 16, 17, 18, 19, 20, 21]. Cluster counting is another useful technique that exploits the volume–redshift relationship and evolution of cluster number density [e.g. 22, 23], although it requires a very good understanding of the distribution of the mass–observable relation including its scatter [24, 25] and the dispersion of the cluster mass function.

The prospects for measuring the dark energy EOS parameters with BAO and WL have been studied in great detail [13, 14, 15, 16, 17, 18, 19, 20, 21, 26, 27, 28, 29, 30, 31, 32, 33, 34, 35, 36, 37, 38, 39, 40, 41, 42, 43, 44]. In the absence of systematic errors and uncertainties of photometric redshift (photo- z) error distribution, a deep and wide multiband WL survey can achieve statistical precisions of ~ 0.1 on the dark energy EOS parameters w_0 and w_a , where the EOS is parametrized as $w = w_0 + w_a(1 - a)$ and a is the scale factor [45]. Shear systematics and uncertainties of photo- z error distribution can severely degrade WL constraints [46, 47, 48, 49]. In addition, the lack of complete understanding of the matter power spectrum on small scales due to nonlinearity and baryonic effects [50, 51, 52, 53, 54] makes it more difficult to fully harness the statistical power of the shear power spectrum on those scales [55].

Given a deep photo- z survey, BAO constraints on w_0 and w_a are generally weaker than those of WL, because the rms photo- z error σ_z filters out radial information on small scales and because we do not have an accurate description of the galaxy clustering bias [21, 31, 32, 36, 44]. When only the auto power spectra are considered, BAO results are sensitive to the uncertainties of the photo- z error distribution [40, 44]. However, the cross power spectra between redshift bins, as we discuss below, can self-calibrate the photo- z bias δz and rms error σ_z . As such, tomographic measurements of BAOs are much less sensitive to the uncertainties of the photo- z error distribution.

Although we treat dark energy phenomenologically with a loose connection to the cosmological constant or quintessence [56, 57, 58, 59], one should bear in mind that dark energy could also be a manifestation of our incomplete knowledge of gravity. For instance, gravity in an extra dimension can accelerate the cosmic expansion [60, 61]. Matching different theories to the same distance–redshift relationship does not guarantee a match of the growth–redshift relationship [20, 62, 63, 64, 65, 66]. Hence, it is important to employ multiple techniques, especially WL, to not only strengthen constraints on dark energy properties but also potentially distinguish between different theories.

We focus on incorporating the two emerging techniques BAO and WL with CMB measurements. Both BAOs and cosmic shear have been recently detected and used to constrain cosmological parameters [67, 68, 69, 70, 71, 72, 73, 74]. More encouragingly, it has been demonstrated that one can achieve an rms photo- z error $\sigma_z \lesssim 0.04(1 + z)$ with deep photometries and sufficient spectroscopic calibrations [75]. With a homogeneous population of luminous red galaxies (LRGs), the rms photo- z error can be even smaller, and the error distribution is fitted well by two Gaussians centred at nearly the same true redshift [76]. This has led to very recent detections of BAO signatures from photo- z LRG samples in the Sloan Digital Sky Survey (SDSS) [77] and MegaZ-LRG catalogue [78] at comparable statistical significance levels as the detections from spectroscopic samples in SDSS [72] and the 2 degree field galaxy redshift survey [73].

To combine BAO with WL in a single survey, one has to properly account for

the galaxy–shear correlation [79]. We further develop the work in [33] to include the uncertainties of the photo- z error distribution and simple additive systematics. Photo- z errors, even if their distribution is known perfectly, degrade cosmological constraints by suppressing the signal. For WL, the lensing kernel itself is much broader than the rms photo- z error σ_z , so that it is not overly sensitive to photo- z errors. However, the uncertainties of the photo- z error distribution introduce uncertainties to the shear signal. Given that future WL surveys can measure shear power spectra to percent level at $\ell \sim 1000$, WL results will be sensitive to the uncertainties of the photo- z error distribution. For BAO, the situation is the opposite. Its kernel is defined by the photo- z error distribution (assuming that the widths of the tomographic bins match the rms photo- z errors), so that BAO power spectra and their cosmological constraints are more sensitive to photo- z errors. But the distinctive dependency of the tomographic galaxy power spectra on photo- z errors is actually an advantage that can be taken to constrain the photo- z error distribution. Consequently, BAO results are less prone to the uncertainties in the photo- z error distribution.

Photo- z errors can have long tails and sometimes can be catastrophically wrong due to the confusion of spectral features (especially the Balmer break for galaxies at $z \lesssim 1$ and the Lyman break for galaxies at $z \gtrsim 2$) or the lack of features in the wavebands [for a review, see 80]. Such catastrophic errors can be mitigated by incorporating galaxy apparent magnitude and size priors or by supplementing near-infrared data [81, 82, 83, 84]. The outliers have been reportedly limited to less than 10% or even completely eliminated in some cases [75, 82, 84, 85].

We idealise the photo- z errors to be Gaussian, so that they can be parametrized with the rms σ_z and bias δz . The Gaussian simplification allows for a pedagogical understanding of the effect of the uncertainties in the photo- z error distribution. The BAO constraints on the photo- z error distribution will be weakened when more parameters are used to model the distribution [86]. However, since WL cannot self-calibrate the photo- z parameters, even very loose error bounds on these parameters from BAO will keep WL constraints on dark energy from being degraded without bound. Spectroscopic calibrations are crucial for both properly modelling the photo- z errors and constraining their distribution, but, it will be very challenging to fairly sample galaxies for spectroscopy over the entire area and depth of future imaging surveys. Therefore, alternative means of constraining the photo- z error distribution, such as photo- z galaxy power spectra [86] and cross-correlations between spectroscopic and photometric galaxy samples [87], will be valuable to these surveys.

Photo- z surveys can be used in many ways to probe the universe, and a single technique can utilise a variety of statistics. We specifically investigate the complementarity between tomographic galaxy and shear power spectra. Higher-order statistics can be very useful [18, 40, 49], but to properly combine them with other statistics, one needs to carefully account for the correlations between different statistics.

The rest of this paper is organised as follows. We define the tomographic galaxy and shear power spectra as well as the CMB power spectra in section 2, and discuss the Fisher information matrix for error estimation in section 3. Our forecasts on cosmological constraints are given in section 4 for four proposed multiband imaging surveys (as far as BAO and WL are concerned): Dark Energy Survey[‡] (DES), Large

[‡] See <http://www.darkenergysurvey.org/>.

Synoptic Survey Telescope§ (LSST), Panoramic Survey Telescope and Rapid Response System|| (PS4), and Supernova/Acceleration Probe¶ (SNAP). We discuss the results and conclude in section 5.

2. Observables

Our observables consist of angular maps of galaxy number density $n(\boldsymbol{\theta})$, shear $\gamma(\boldsymbol{\theta})$, and CMB temperature and polarisation fluctuations. The tomographic galaxy and shear power spectra are the covariance of galaxy number density and shear in Fourier space, as are the CMB temperature and polarisation power spectra to temperature and polarisation. In what follows, we loosely refer to these power spectra as observables as well, despite that using power spectra as true observables in the forecast requires a slightly different formalism.

2.1. Galaxy and shear power spectra

With the Limber approximation [88, 89], the angular power spectrum of $n(\boldsymbol{\theta})$ and $\gamma(\boldsymbol{\theta})$ can be written as [33]

$$P_{ij}^{XY}(\ell) = \frac{2\pi^2}{c\ell^3} \int dz H(z) D_A(z) W_i^X(z) W_j^Y(z) \Delta_\delta^2(k; z), \quad (1)$$

where lower case subscripts correspond to the tomographic bins, upper case superscripts label the observables, i.e., $X = g$ for galaxies or γ for shear, $H(z)$ is the Hubble parameter, $D_A(z)$ is the comoving angular diameter distance, $\Delta_\delta^2(k; z)$ is the dimensionless power spectrum of the density field, and $k = \ell/D_A(z)$. BAO and WL do not necessarily use the same binning. In other words, the bin number is defined for each technique separately. The window function is

$$W_i^X(z) = \begin{cases} b(z) \frac{n_i(z)}{\bar{n}_i} & X = g \\ \frac{3}{2} \frac{\Omega_m H_0^2}{H(z)} \frac{D_A(z)}{a c} \int_z^\infty dz' \frac{n_i(z')}{\bar{n}_i} \frac{D_A(z, z')}{D_A(z')} & X = \gamma, \end{cases} \quad (2)$$

where $b(z)$ is the linear galaxy clustering bias, and Ω_m and H_0 are, respectively, the matter fraction at $z = 0$ and Hubble constant. The galaxy redshift distribution $n_i(z)$ in the i th tomographic bin is an average of the underlying three-dimensional galaxy distribution over angles, and the mean surface density \bar{n}_i is the total number of galaxies per steradian in bin i . The distribution $n_i(z)$ is broader than the nominal width of the tomographic bin (defined in photo- z space) because of photo- z errors.

We only include galaxy power spectra on largely linear scales, e.g., the scales of BAOs, in our analysis, so that we can map the matter power spectrum to galaxy power spectrum with a scale-independent but time-evolving linear galaxy bias [90, 91]. One may extend the analysis to smaller scales with a halo model to describe the scale dependency of the galaxy bias and, in fact, can still constrain the scale-dependent galaxy bias to 1% level [33].

Cast in the form of (1) and (2), it seems as though the WL kernel $W_i^\gamma(z)$ is sensitive to the matter fraction Ω_m (or the matter density $\omega_m = \Omega_m h^2$, where h is

§ See <http://www.lsst.org/>.

|| See <http://pan-starrs.ifa.hawaii.edu/>.

¶ See <http://www.snap.lbl.gov/>. As its name suggests, SNAP is also designed to measure SN redshifts with spectroscopy.

the Hubble constant in units of $100 \text{ km s}^{-1} \text{ Mpc}^{-1}$). Potential (or spatial curvature) perturbations, for which inflation often predicts a nearly scale-invariant behaviour, are more fundamental than density perturbations. WL shear and CMB temperature fluctuations are also driven directly by the fluctuations in the gravitational potential rather than the density. Therefore, we recast the angular power spectra in terms of the potential power spectrum:

$$P_{ij}^{XY}(\ell) = \frac{2\pi^2\ell}{c} \int dz H D_A W_i^X W_j^Y \Delta_\phi^2(k), \quad (3)$$

with

$$W_i^X = \begin{cases} \frac{n_i}{\bar{n}_i} \frac{2ab}{3\Omega_m H_0^2 D_A^2} & X = g \\ \frac{1}{c H D_A} \int_z^\infty dz' \frac{n_i(z')}{\bar{n}_i} \frac{D_A(z, z')}{D_A(z')} & X = \gamma. \end{cases} \quad (4)$$

We have dropped the argument z in (3) and (4) where there is no confusion. One may choose to normalise to either the density, e.g., the rms density fluctuation σ_8 within a radius of $8 h^{-1} \text{ Mpc}$ at $z = 0$, or the potential, e.g., the CMB temperature power spectra, but one should propagate the factors of ω_m through to ensure that gravitational lensing responds to potential directly. Moreover, precise measurements of CMB power spectra have made it more desirable as well as convenient to normalise to the potential fluctuations.

Observationally, the power spectra will have contributions from galaxy shot (shape) noise \bar{n}_i^{-1} ($\gamma_{\text{rms}}^2 \bar{n}_i^{-1}$) and systematic noise N_{sys}^X :

$$\tilde{P}_{ij}^{XY}(\ell) = P_{ij}^{XY}(\ell) + \delta_{XY}^K \left(N_{\text{sys}}^X + \delta_{ij}^K \frac{X_{\text{rms}}^2}{\bar{n}_i} \right), \quad (5)$$

where δ_{XY}^K and δ_{ij}^K are Kronecker delta functions. For galaxies, $g_{\text{rms}} \equiv 1$, and, for the shear, $\gamma_{\text{rms}} \sim 0.2$ is due to the intrinsic shape of galaxies and measurement errors. The systematic noise N_{sys}^X may arise from (the residuals after correcting for) the spatially varying dust extinction, photometry offsets, point spread function (PSF), instrumentation effects, and so on [92, 93, 94]. We have assumed in (5) that N_{sys}^X is additive, uncorrelated between BAO and WL, and independent of tomographic bins or multipoles. This is a great simplification over the additive errors considered in [49], which shows that the degradation to WL results by the systematics is generally not bound. The systematic noise we include is among a sub-set of (unrealistic) additive errors whose degradation effect can be shown mathematically to be less than $\sim 100\%$ [49]. As such, we have effectively made an aggressive assumption that all other types of systematics are well under control.

Previous forecasts for BAO use only the three or two-dimensional galaxy auto power spectrum within each redshift bin [29, 31, 32, 35, 36, 40, 43, 44]. This is a good approximation for spectroscopic surveys, because the intrinsic correlation (due to the large-scale structure) between two redshift bins is small if the bins are wide enough. For photo- z surveys, the cross-bin power spectra $P_{ij}^{\text{gg}}(\ell)$ are no longer negligible due to photo- z errors. The left panel of figure 1 shows that $P_{ij}^{\text{gg}}(\ell)$ (broken lines), depending on the binning and photo- z errors, can have comparable amplitudes to that of the auto power spectrum $P_{ii}^{\text{gg}}(\ell)$ (solid line). Not including the covariance between observables in different bins, i.e., the cross power spectra, generally leads to more optimistic error estimates.

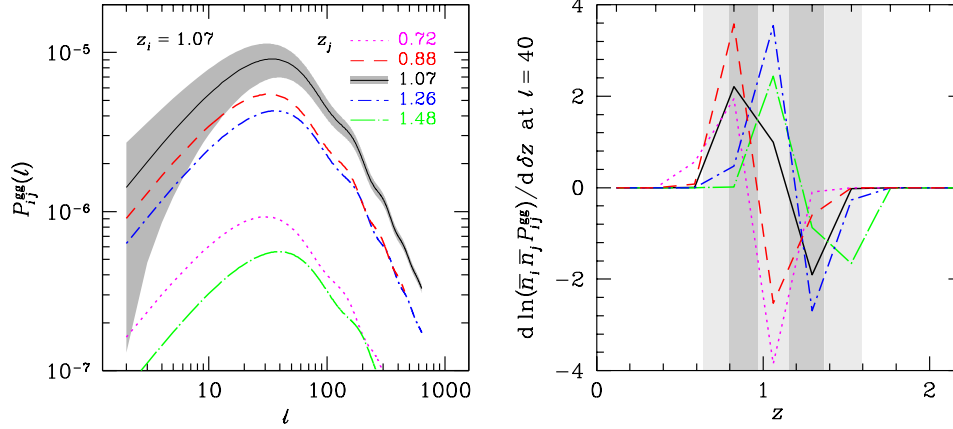


Figure 1. *Left panel:* Angular galaxy power spectra $P_{ij}^{gg}(\ell)$ with bin i centred at $z_p = 1.07$ and bin j centred at $z_p = 0.72$ (dotted line), 0.88 (dashed line), 1.07 (solid line), 1.26 (dash-dotted line), and 1.48 (long-dash-dotted line). The shaded area indicates 1σ statistical errors of the auto power spectrum $\Delta P_{ii}^{gg}(\ell) = [(\ell + 0.5)f_{\text{sky}}]^{-1/2} \tilde{P}_{ii}^{gg}(\ell)$, where f_{sky} is the sky coverage, for LSST. The right end of each power spectrum curve is set by an ℓ_{max} for each tomographic bin to reduce contaminations from nonlinearity. *Right panel:* Sensitivity of the observables $\bar{n}_i \bar{n}_j P_{ij}^{gg}(\ell)$ to the photo- z bias δz . The derivatives are evaluated at $\ell = 40$ to avoid contributions from baryon oscillations that are prominent at $\ell \gtrsim 100$. Though not shown, $\bar{n}_i \bar{n}_j P_{ij}^{gg}(\ell)$ is also sensitive to the photo- z rms error. The grey vertical bands correspond to the relevant tomographic bins in photo- z space, while the upper ticks mark the positions of photo- z parameters in true redshift space. For demonstration purpose, we use 15 tomographic bins from $z_p = 0.15$ to 3.5 in photo- z space and 17 photo- z parameters uniformly distributed from $z = 0$ to 4 in true redshift space. The widths of the bins are proportional to $(1 + z_p)$.

Aside from statistical necessity, tomographic galaxy power spectra will also be very useful for parameter estimation with photo- z BAO experiments, because they provide valuable information about photo- z errors. The reason is that, with Limber approximation, the cross power spectra $P_{ij}^{gg}(\ell)$ are determined by the overlap of galaxy number density distributions n_i and n_j in true redshift space and thus sensitive to photo- z bias δz and rms error σ_z . This is demonstrated in the right panel of figure 1, where derivatives of the new observables⁺ $\bar{n}_i \bar{n}_j P_{ij}^{gg}(\ell)$ with respect to photo- z bias parameters (see section 3 for details) are given at $\ell = 40$. The extents of the relevant tomographic bins are indicated by grey vertical bands, and the locations of the photo- z parameters are marked by upper ticks. The photo- z bias at an arbitrary redshift is linearly interpolated between two photo- z bias parameters.

We refer to the galaxy bin centred at $z_p = 1.07$ (the subscript p following z signifies photo- z s) as bin i in the following discussion. An increase of the photo- z bias δz at $z = 0.82$ means that the redshifts of galaxies around $z = 0.82$ are more likely to be overestimated. As a result, more of these galaxies will be assigned to bin i . With no change to the contributions of galaxies from other redshifts, the auto power spectrum $\bar{n}_i^2 P_{ii}^{gg}$ (solid line) increases correspondingly. The product of the fiducial

⁺ It is argued in [48] that $\bar{n}_i \bar{n}_j P_{ij}^{\gamma\gamma}(\ell)$ is the fundamental observable for WL. Our forecasts for cosmological parameters are not affected by this change of observables, but the constraints on photo- z parameters are slightly improved.

galaxy clustering bias and linear growth function evolves less than 1% in this redshift range, so that the change in the mixing of galaxy number fluctuations at different redshift is sub-dominant to the effect of increased \bar{n}_i . Similarly, an increase of δz at $z = 1.29$ leads to fewer $z \sim 1.29$ galaxies assigned to bin i and thus lowers $\bar{n}_i^2 P_{ii}^{\text{gg}}$.

The behaviour of the auto power spectrum $\bar{n}_i^2 P_{ii}^{\text{gg}}$ as a function of the photo- z bias δz near the nominal centre of bin i depends on the overall galaxy distribution $n(z)$. An increase of δz at $z = 1.06$ (by linear interpolation, it increases the photo- z bias in the range $0.82 < z < 1.29$) will shift some galaxies from bin $i - 1$ to bin i and some from bin i to bin $i + 1$. Since the fiducial $n(z)$ peaks at $z = 1$, the net result is more galaxies in bin i and, hence, a positive response of $\bar{n}_i^2 P_{ii}^{\text{gg}}$ to δz at $z = 1.06$.

The cross power spectra are more sensitive to the tail of the photo- z error distribution, because they are determined by the overlap between two tomographic bins in true redshift space. Although the increase of δz at $z = 0.82$ leads to fewer galaxies in lower-redshift bins (dotted line and dashed line), the increased overlap between these bins and bin i , i.e., bin i getting more $z \sim 0.82$ galaxies, results in a boost to $\bar{n}_i \bar{n}_j P_{ij}^{\text{gg}}$ for $j < i$. The increase of δz at $z = 1.06$ reduces the number of $z \sim 1.06$ galaxies assigned to the lower-redshift bins, so that $\bar{n}_i \bar{n}_j P_{ij}^{\text{gg}}$ decreases. The behaviour of the cross power spectra between higher redshift bins and bin i (dash-dotted line and long-dash-dotted line) can be explained similarly.

For our forecasts, we use CMBFAST version 4.5.1 [95] to calculate the matter transfer function at $z = 0$, and then apply the linear growth function and Peacock & Dodds fitting formula (PD96) [96] to obtain the nonlinear matter power spectrum at any redshift. Details are given in Appendix A and Appendix B. To reduce contaminations of the small-scale nonlinearity and baryonic effects [32, 37, 38, 50, 51, 52, 53, 54], we set a smallest angular scale in our analysis. Separately, to avoid possible effects of dark energy clustering that have not been considered in our analysis, we also discard galaxy and shear statistics on very large angular scales [19]. This limits the multipoles $40 \leq \ell \leq 2000$ for WL. The BAO kernel is rather narrow, so it is more appropriate to set the criterion in k space. We require that the dimensionless power spectrum $\Delta_\delta^2(k; z) < 0.4$ in each tomographic bin *and* that $40 \leq \ell \leq 3000$ for BAO. The maximum multipole for a galaxy bin centred at z_p follows approximately $\ell_{\text{max}} = 340z_p + 346z_p^2$ at $0.15 \leq z_p \leq 0.9$, $446 - 658z_p + 908z_p^2$ at $0.9 < z_p \leq 2.1$, and 3000 at $z_p > 2.1$. Setting the minimum multipole to 100 or reducing the maximum multipole by 1000 for both BAO and WL does not severely impact our forecasts (see section 5).

2.2. Cosmic microwave background

CMB temperature and polarisation power spectra are calculated with CMBFAST for scalar modes:

$$\mathcal{C}_\ell^{XY} = 2(2\pi)^4 \int d \ln k \Delta_\phi^2(k) \Delta_\ell^X(k) \Delta_\ell^Y(k), \quad (6)$$

where $X = \text{T}$ for temperature or E for E-polarisation, and $\Delta_\ell^X(k)$ is the radiation transfer function [97]. With noise, the power spectra become

$$\tilde{\mathcal{C}}_\ell^{XY} = \mathcal{C}_\ell^{XY} + \delta_{XY}^{\text{K}} \left(\sum_i \theta_{\text{b},i}^{-2} X_{\text{rms},i}^{-2} B_{\ell,i}^2 \right)^{-1}, \quad (7)$$

where $\theta_{\text{b},i}$ is the full width half-maximum of the beam in channel i , $X_{\text{rms},i}$ is the noise per pixel in temperature or polarisation measurements, and $B_{\ell,i}$ is the beam window

function [97, 98]. We model the CMB experiment after *Planck* with instrumental characteristics tabulated in [99]. We assume a sky fraction of $f_{\text{sky}} = 0.8$ after a foreground cut, and limit the multipoles $2 \leq \ell \leq 2000$ for temperature and $10 \leq \ell \leq 2500$ for polarisation.

CMB temperature and polarisation are nearly uncorrelated with the galaxy distribution except for the late-time integrated Sachs-Wolfe (ISW) effect on large angular scales [100]. Since we do not use BAO or WL at $\ell < 40$, it is straightforward to combine CMB with BAO and WL.

3. Error estimation

Assuming that the likelihood function of the true observables, e.g., the map data, is approximately a multivariate Gaussian around the maximum, one can use the Fisher information matrix to estimate the lower bound of errors of the parameters that could be inferred [101, 102, 103, 104].

3.1. Fisher matrix

The Fisher matrix of parameters $\{p_\alpha\}$ is given by [104]

$$F_{\alpha\beta} = \frac{1}{2} \text{Tr} \mathbf{C}^{-1} \frac{\partial \mathbf{C}}{\partial p_\alpha} \mathbf{C}^{-1} \frac{\partial \mathbf{C}}{\partial p_\beta} + \frac{\partial \boldsymbol{\mu}^T}{\partial p_\alpha} \mathbf{C}^{-1} \frac{\partial \boldsymbol{\mu}}{\partial p_\beta}, \quad (8)$$

where \mathbf{C} and $\boldsymbol{\mu}$ are, respectively, the covariance and mean of the true observables. For our purpose, the observables have zero mean, and the contributions to the Fisher matrix from different spherical harmonic modes are separable, so that

$$F_{\alpha\beta} = f_{\text{sky}} \sum_{\ell} \frac{2\ell+1}{2} \text{Tr} \mathbf{C}_\ell^{-1} \frac{\partial \mathbf{C}_\ell}{\partial p_\alpha} \mathbf{C}_\ell^{-1} \frac{\partial \mathbf{C}_\ell}{\partial p_\beta}, \quad (9)$$

with $(\mathbf{C}_\ell)_{ij}^{XY} = \tilde{P}_{ij}^{XY}(\ell)$ for galaxies and shear (BAO+WL), and $(\mathbf{C}_\ell)^{UV} = \tilde{C}_\ell^{UV}$ for CMB. The factor f_{sky} approximates the effect of incomplete sky coverage with a reduction of modes. This is valid for a contiguous survey with roughly the same angular size in all directions. The total Fisher matrix is a direct sum of the BAO+WL and CMB Fisher matrices.

Equation (9) can be reduced to

$$F_{\alpha\beta} = f_{\text{sky}} \sum_{\ell} (2\ell+1) \frac{\partial \mathbf{Q}_\ell^T}{\partial p_\alpha} \mathbf{M}_\ell^{-1} \frac{\partial \mathbf{Q}_\ell}{\partial p_\beta}, \quad (10)$$

where \mathbf{Q}_ℓ is a column vector containing unique elements of \mathbf{C}_ℓ , and \mathbf{M}_ℓ equals the covariance of \mathbf{Q}_ℓ in the Gaussian case [33]. From (10), it may seem possible to discard the cross power spectra in error forecasts. However, the Fisher matrix (8) and (10) are based on the multivariate Gaussian likelihood of the true observables, e.g.,

$$-2 \ln \mathcal{L}(\mathbf{n}_\ell) = \ln |\mathbf{C}_\ell^{\text{gg}}| + \mathbf{n}_\ell^T (\mathbf{C}_\ell^{\text{gg}})^{-1} \mathbf{n}_\ell + \text{const}, \quad (11)$$

where \mathbf{n}_ℓ is a column vector of the galaxy angular distribution in multipole space, whereas the likelihood becomes

$$-2 \ln \mathcal{L}'(\mathbf{n}_\ell) = \sum_i \left[\ln C_{ii,\ell}^{\text{gg}} + n_{i,\ell}^2 (C_{ii,\ell}^{\text{gg}})^{-1} \right] + \text{const}, \quad (12)$$

if the cross power spectra are discarded. The two likelihood functions \mathcal{L} and \mathcal{L}' can differ considerably, when, for instance, photo- z errors induce strong correlations of

the galaxy number density fluctuations between the bins. Discarding the correlations between the observables may lead to underestimation of the errors on cosmological parameters [e.g., 105]. However, in the case of BAO, the galaxy cross power spectra are crucial for calibrating the photo- z error distribution, which is, in turn, critical to measuring the dark energy EOS parameters accurately with the WL technique. Consequently, the joint BAO and WL constraints on dark energy can be weakened if one does not utilise the galaxy cross power spectra (see the footnote of table 3).

To use the power spectra as true observables, one can replace $\boldsymbol{\mu}$ and \boldsymbol{C} in (8) with the power spectra and their covariance, respectively. In doing so, one also assumes that the likelihood function of the power spectra is a multivariate Gaussian, which is generally not the same as assuming a Gaussian likelihood function for the map data.

3.2. Parameters

Our parameter set includes 11 cosmological parameters, 40 galaxy bias parameters, 40 photo- z bias parameters, 40 photo- z rms parameters, one systematic noise parameter for BAO, and one systematic noise parameter for WL. There are 133 parameters in total for the joint BAO and WL analysis. When the BAO and WL techniques are considered separately, their respective irrelevant parameters are held fixed.

The cosmological parameters are the dark energy EOS parameters w_0 and w_a , the matter density ω_m , the baryon density ω_b , the angular size of the sound horizon at the last scattering surface θ_s , the equivalent matter fraction of curvature Ω_K , the optical depth τ to scattering by electrons in the reionized intergalactic medium, the primordial helium mass fraction Y_p , the spectral index n_s of the primordial scalar perturbation power spectrum, the running of the spectral index α , and the normalisation of the primordial curvature power spectrum Δ_R^2 (or $\frac{25}{9}\Delta_\phi^2$ in matter era) at $k = 0.05 \text{ Mpc}^{-1}$. We adopt the three-year *WMAP* results [9] for fiducial values of the parameters: $(w_0, w_a, \omega_m, \omega_b, \theta_s, \Omega_K, \tau, Y_p, n_s, \alpha, \Delta_R^2) = (-1, 0, 0.127, 0.0223, 0.596^\circ, 0, 0.09, 0.24, 0.951, 0, 2.0 \times 10^{-9})$. The reduced Hubble constant $h = 0.73$ and the present equivalent matter fraction of dark energy $\Omega_X = 0.76$ are implicit in our parametrization.

The photo- z bias and rms error parameters are implemented according to [48]; we evenly space the parameters from $z = 0$ to 4 and linearly interpolate the values at arbitrary redshifts. Note that the photo- z parameters are assigned in true-redshift space and that they are not attached to any galaxy or shear bins. The galaxy clustering bias is parametrized in the same way. This scheme is based on the expectation that photo- z s and the galaxy bias behave more or less smoothly from one redshift to another. It is found that the WL forecasts for a DES-like survey become roughly convergent when the redshift interval of the photo- z parameters is less than 0.15 [48]. The convergent redshift interval may be different for other surveys, but it will be very expensive to achieve the same precision of the photo- z calibration via spectroscopy at a much finer interval. We expect that ambitious photo- z calibrations will be carried out at ~ 0.1 redshift intervals (LSST photo- z calibration white paper*) and that similar measurements of the galaxy clustering bias will be available. This amounts to 40 parameters each for the galaxy bias, photo- z bias, and photo- z rms over $0 \leq z \leq 4$. The actual calibration requirement may be less stringent if one combines BAO with WL (see section 4). The photo- z and galaxy clustering bias parameters extend beyond the nominal cut-off (photometric) redshift of the surveys to accommodate the galaxy distribution of the last tomographic bin in true redshift space. Our forecasts are

* See <http://www.lsst.org/Science/Phot-z-plan.pdf>.

Table 1. Priors and additive systematics ^a.

Case	$\sigma_P(\delta z)^b$	$\sigma_P(\ln b)$	N_{sys}^g	N_{sys}^γ
Opt.	$0.05 \sigma_z$	0.15	10^{-8}	10^{-8}
Pes.	$0.2 \sigma_z$	0.3	2×10^{-7}	2×10^{-7}

^a The additive systematic errors are defined in (5).^b $\sigma_P(\sigma_z) = \sqrt{2}\sigma_P(\delta z)$.

not affected by this extension, because the low galaxy number density and poor measurements reduce the statistical significance of the data around the cut-off redshift.

We assume $b = 1 + 0.84z$ [106], $\delta z = 0$, and $\sigma_z \propto (1+z)$ for the fiducial model. The galaxy distribution n_i in each tomographic bin is determined from the overall galaxy redshift distribution $n(z)$ and photo- z parameters

$$n_i = n(z)P(z_{p,i}^B, z_{p,i}^E; z) = n(z)I(z_{p,i}^B, z_{p,i}^E; z)/I(0, \infty; z), \quad (13)$$

where $z_{p,i}^B$ and $z_{p,i}^E$ define the extent of bin i , and $P(z_{p,i}^B, z_{p,i}^E; z)$ is the probability of assigning a galaxy that is at true redshift z to bin i . The unnormalised probability $I(a, b; z)$ is given by [48]

$$I(a, b; z) = \frac{1}{\sqrt{2\pi}\sigma_z} \int_a^b dz_p \exp \left[-\frac{(z_p - z - \delta z)^2}{2\sigma_z^2} \right], \quad (14)$$

and the normalisation $I(0, \infty, z)$ is enforced because photo- z s are non-negative. Note that even though the probability distribution of photo- z s at a given true redshift is assumed Gaussian, the reverse is not true. In other words, the Gaussian assumption is flexible enough to allow for modelling of more complex galaxy distributions in tomographic bins [48].

The derivatives in (10) are taken two-sided numerically with steps in parameters $\Delta(w_0, w_a, \omega_m, \omega_b, \theta_s, \Omega_K, \tau, Y_p, n_s, \alpha) = \pm 10^{-3} \times (20, 40, 6, 1, 3, 10, 10, 20, 5, 5)$. The derivative with respect to Δ_R^2 is analytic. The steps of the galaxy clustering bias parameters are $\pm 0.005b$, and those of the photo- z parameters are $\pm 0.005(1+z)$. When differentiating with respect to the photo- z parameters, we keep the overall underlying distribution of galaxies, i.e., $n(z)$, invariant, because the true redshift of a galaxy cannot be affected by photo- z algorithms. This approach is complementary to that of [40, 44, 49, 86], in which the number of galaxies in each tomographic bin is fixed or tightly constrained while $n(z)$ is allowed to vary. The two approaches are found to be consistent for WL [49]. For BAO, $n(z)$ will be largely degenerate with the galaxy clustering bias. Given that our BAO results on the galaxy bias are roughly consistent with those in [40], which achieve $\sim 2\%$ constraints for a $z < 1.3$ and $f_{\text{sky}} = 0.1$ survey with $\sigma_P(\delta z) = 0.01(1+z)$, the two approaches can be consistent for BAO as well.

We treat the additive systematics of BAO and WL as nuisance parameters. Since they can be determined very well from the data, the additive systematics affect the constraints mostly by boosting the covariance [49]. Our forecasts will not improve even if N_{sys}^g and N_{sys}^γ are fixed. This is somewhat misleading, because even a very slight modification to the form of the systematics can lead to unrestrained degradation to cosmological constraints for WL [49]. Therefore, one must adequately calibrate and control all sorts of systematics in order to achieve the constraints we forecast.

We incorporate independent measurements of galaxy bias and photo- z parameters as Gaussian priors in the Fisher matrix. Since the results depend on these priors and

Table 2. Survey specifications.

Survey	Area deg ²	Filters	Depth r mag (10σ)	\bar{n} arcmin ⁻²	z^*	σ_z ($1+z$)
DES	5000	<i>griz</i>	24.1	8	0.3	0.07
LSST	20000	<i>ugrizy</i>	26.5	50	0.5	0.05
PS4	20000	<i>grizy</i>	24.1	8	0.3	0.07
SNAP	1000	9 bands ^a	26.6	100	0.7	0.04

^a From optical to near-infrared.

the systematics to some degree, we list our assumptions in table 1 for both pessimistic and optimistic cases. Note that we use a subscript P for priors, i.e., $\sigma_P(p_\alpha)$, to distinguish them from constraints $\sigma(p_\alpha)$. For Gaussian photo- z errors, a prior of $\sigma_P(\delta z) = 0.05\sigma_z$ translates to 400 fairly sampled spectra for calibration around the redshift of the photo- z bias parameter. Current determination of the galaxy clustering bias is at 10% level for low redshift galaxies [90, 107, 108]. This may or may not be achievable at higher redshift, but it is not critical as BAO and WL, along with CMB, can determine the galaxy clustering bias quite well.

We infer from the systematic errors (including extinction, photometry calibration, and seeing) of the SDSS angular galaxy power spectrum [92] that $10^{-8} \lesssim N_{\text{sys}}^g \lesssim$ a few 10^{-7} . For WL, the specified systematic shear noise is somewhat arbitrary and perhaps conservative, because its amplitude is relatively high compared to that of the shear power spectra. This partially compensates the fact that we restrict N_{sys}^γ to a very simple additive form. We also note that the effect of the simple noise N_{sys}^γ saturates quickly at $N_{\text{sys}}^\gamma \gtrsim$ a few 10^{-8} [49]. In what follows, we assume the optimistic case by default, and the pessimistic results are presented in table 4.

4. Forecasts

The puzzle of dark energy has inspired a number of ambitious photometric and spectroscopic surveys that are proposed to unravel the mystery via multiple techniques. Among them, we choose to forecast cosmological constraints of BAO and WL for four multiband imaging surveys: DES, LSST, PS4, and SNAP in conjunction with CMB measurements by *Planck*, which is always included. It should be noted that all the four surveys propose to utilise one or two other techniques, SN and cluster counting, to constrain cosmology, and that BAO and/or WL may not even be their primary dark energy probe.

We use the error product (EP)

$$\sigma(w_p) \times \sigma(w_a) = [\sigma^2(w_0)\sigma^2(w_a) - \text{Cov}^2(w_0, w_a)]^{1/2}, \quad (15)$$

where $\text{Cov}(w_0, w_a)$ is the covariance between w_0 and w_a , to assess dark energy constraints throughout this section. The minimum error of the dark energy EOS $\sigma(w_p)$ is achieved at the pivot expansion factor

$$a_p = 1 + \text{Cov}(w_0, w_a)/\sigma^2(w_a) \quad (16)$$

and is equal to the error on w_0 with w_a held fixed [33, 98, 109]. This product is proportional to the area of the error ellipse in the w_0 - w_a plane and inversely proportional to the figure of merit used by the Dark Energy Task Force.

4.1. Surveys

We model the underlying galaxy redshift distribution with

$$n \propto z^2 e^{-z/z^*}, \quad (17)$$

which is in good agreement with photometry simulations based on degraded Hubble Deep Field North images [110]. The normalisation is adjusted to match the total surface density of galaxies \bar{n} , and the galaxy distribution peaks at $2z^*$. Specifications of the four surveys are listed in table 2.

Following [19], we adopt a redshift-dependent rms shear

$$\gamma_{\text{rms}} = 0.18 + 0.042 z \quad (18)$$

for all the surveys. Smaller rms shear may be achieved with a subsample of well measured galaxies, and one can optimise the trade between γ_{rms} and n_i to reduce the shape noise $\gamma_{\text{rms}}^2 n_i^{-1}$ for WL. It can also be beneficial to weight galaxies differently based on their measurement quality such as that of the shape noise and photo- z to optimise cosmological constraints.

4.2. Dark energy constraints from BAO and WL separately

The binning of the data affects the amount of information one can extract from the survey. Due to its broad kernel, WL only requires a small number of tomographic bins to fully reach its potential. For DES, five bins are sufficient [48]. We use 10 equal-width WL bins from $z_p = 0$ to 3.5 for all the surveys. BAO, on the other hand, has narrow kernels that are defined by the galaxy distribution n_i , so that one can continue to extract information with finer bins until shot noise overwhelms the signal or the bin widths are less than the rms photo- z error.

Figure 2 presents the EP as a function of the number of BAO bins for each survey without the systematic noise, which can only reduce the number of bins required. We set the width of the bins to be proportional to $(1 + z_p)$ to match the rms photo- z error. As expected, one can improve the dark energy constraint by using more tomographic bins until it saturates. The point of saturation depends on the depth of the survey and σ_z . For LSST (solid line) and SNAP (dotted line), the EP of 40 bins is only 7% worse than that of 90 bins, so, hereafter, we use 40 BAO bins for all the surveys. With uniform BAO bins (open circles), the EP is more sensitive to the number of bins used. This suggests that it may be useful to optimise the tomographic binning for BAO. One possibility is to evenly distribute the (auto power spectrum) signal to noise ratio for each bin.

BAO and WL, individually, are subject to different systematics and parameter uncertainties, but their combination can be substantially more robust. We first quantify in figure 3 the effect of the photo- z prior and fiducial value of the additive systematic noise on LSST BAO (left panel) and WL (right panel) using the EP. The BAO EP varies slowly with $\sigma_P(\delta z)$ and N_{sys}^g , because LSST BAO is capable of self-calibrating the photo- z parameters to $10^{-3}(1 + z)$ level (see figure 4) and the BAO systematic noise is fairly low compared to the galaxy power spectra. WL is unable to constrain the photo- z parameters, so that it is sensitive to the photo- z prior on $\sigma_P(\delta z)$. The degradation to WL EP caused by the shear systematic noise saturates when $N_{\text{sys}}^\gamma \gtrsim$ a few 10^{-8} , which is consistent with [49]. Figure 3 demonstrates that to take the advantage of the WL technique one needs to know the photo- z error distribution accurately and have adequate control over the shear systematics.

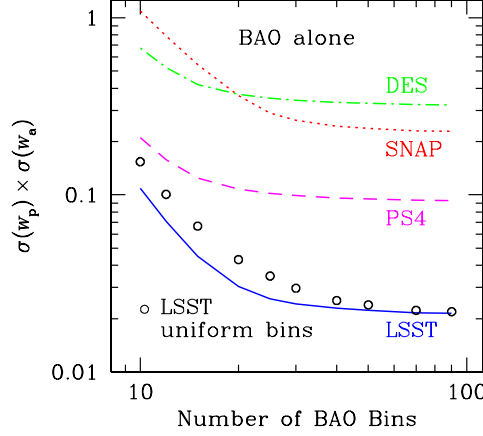


Figure 2. The EP, $\sigma(w_p) \times \sigma(w_a)$, of BAO as a function of the number of tomographic bins for the four proposed surveys: DES (dash-dotted line), LSST (solid line), PS4 (dashed line), and SNAP (dotted line). The results are calculated without varying the number of parameters for the galaxy bias, photo- z bias, and photo- z rms, because they are defined in true-redshift space regardless the binning of galaxies in photo- z space. The bin widths are proportional to $(1 + z_p)$ except that open circles are obtained with equal-size bins for LSST. The constraints are evaluated for the optimistic case in table 1 but without the systematic error, which slightly reduces the number of bins needed to fully extract cosmological information from galaxy power spectra.

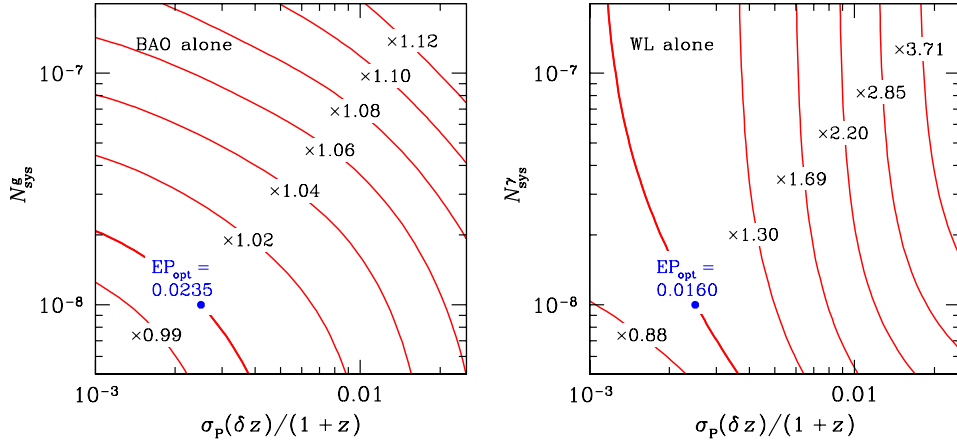


Figure 3. *Left panel:* Contours of the EP, $\sigma(w_p) \times \sigma(w_a)$, of LSST BAO as a function of the prior of the photo- z parameters and fiducial value of the simple additive systematic noise. To reduce the dimension of the parameter space, we set the prior on the rms photo- z errors to $\sigma_P(\sigma_z) = \sqrt{2} \sigma_P(\delta z)$. The solid dot locates at the coordinates specified by the optimistic values of $\sigma_P(\delta z)$ and N_{sys}^g . *Right panel:* Same as the left panel, but for LSST WL. Notice that the EP of LSST WL varies by a factor of 5.9 across the ranges of the photo- z prior and systematic noise shown (from the lower left corner to the upper right corner), whereas the EP of LSST BAO changes by only 18%. If $N_{sys}^g = N_{sys}^\gamma = 0$ and $\sigma_P(\delta z)$ remains the same as that in the optimistic case, one could achieve $EP = 0.0231$ and 0.0068 with BAO and WL, respectively.

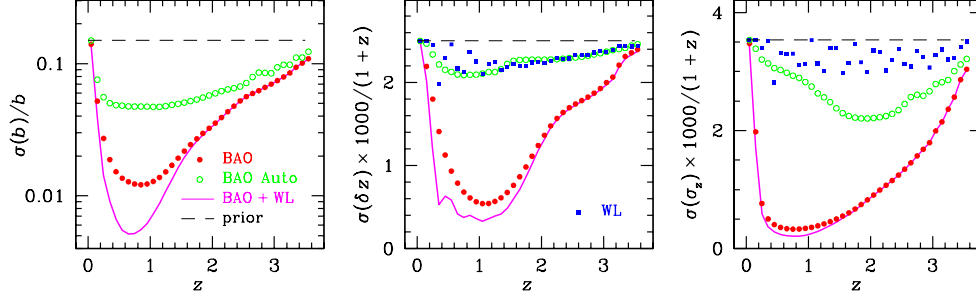


Figure 4. *Left panel:* Constraints on the galaxy clustering bias parameters from LSST BAO (with both the auto and cross power spectra, solid circles), BAO with the auto power spectra only (open circles), and joint BAO and WL (solid line). The 15% prior on each parameter is drawn in a thin dashed line. The constraints are tightest near $z = 1$, roughly corresponding to the peak of the overall galaxy distribution. *Middle panel:* Constraints on the photo- z bias parameters. The legends are the same as in the left panel with the addition of LSST WL in solid squares. The prior is taken to be $\sigma_P(\delta z) = 0.05\sigma_z = 0.0025(1+z)$. *Right panel:* Same as the middle panel, but for the photo- z rms parameters. The prior is a factor of $\sqrt{2}$ weaker than that on δz . The galaxy cross power spectra are indeed crucial for self-calibrating the photo- z parameters and constraining the galaxy clustering bias. The oscillatory behaviour of WL constraints is caused by the offsets between the photo- z parameters and each tomographic bin.

For BAO, the linear galaxy clustering bias b is degenerate with the linear growth function G . Therefore, one cannot extract much useful information from the growth of the large-scale structure with BAO. It may seem contradictory from the left panel of figure 4 that the galaxy bias b (and, hence, the growth G) can actually be determined to several percent with BAO (solid circles). This is made possible by normalising the matter power spectrum to the precisely measured CMB fluctuations so that the difference between the galaxy and extrapolated matter power spectrum at low redshift gives the galaxy bias directly. Even though the error of the galaxy bias can be as small as a few percent, it is still not a match to that of the distance from BAO [32, 44]. Without the galaxy cross power spectra (open circles), the BAO results become several times worse, showing that the cross power spectra are useful for constraining the galaxy bias. Since WL is not affected by the galaxy bias, its combination with BAO (solid line) improves $\sigma(b)$ significantly. The tightest constraint on b occurs at a redshift that is lower than the peak of the overall galaxy distribution, because WL kernel peaks below the redshift of source galaxies.

BAO and WL constraints on the photo- z parameters δz and σ_z are shown, respectively, in the middle and right panels of figure 4. One sees that WL (solid squares) does not have much control on the photo- z parameters because of its broad kernel, while BAO, with both the auto and cross power spectra, is capable of calibrating the parameters to $10^{-3}(1+z)$ level. The galaxy cross power spectra play an important role in the BAO self-calibration of the photo- z error distribution; without them, the BAO constraints on the photo- z parameters become much weaker. Figure 4 thus explains the markedly different response to the photo- z bias prior between the BAO and WL EPs in figure 3. It should be emphasised that the BAO self-calibration of the photo- z parameters cannot replace spectroscopic calibrations, because, without knowing how to faithfully parametrize the photo- z error distribution,

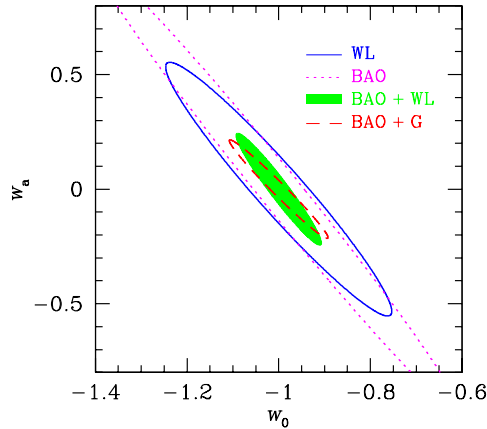


Figure 5. Complementarity between BAO and WL. The 1σ w_0 - w_a contours are shown for LSST BAO (dotted line), LSST WL (solid line), joint BAO and WL (shaded area), and the case of BAO plus growth information (dashed line), for which we fix the galaxy clustering bias parameters to their fiducial values. The last case is unrealistic, but it demonstrates the importance of the growth information.

the self-calibration will be less useful.

The photo- z constraints are much tighter than those of the galaxy clustering bias. The reasons are that the galaxy power spectra are more sensitive to the photo- z parameters than to the galaxy bias and that the dependence of the galaxy power spectra on the photo- z parameters is very unique. For instance, the derivative $d \ln \bar{n}_i \bar{n}_j P_{ij}^{gg} / db$ is roughly unity at $z \sim 1$ for all i and j , whereas $d \ln \bar{n}_i \bar{n}_j P_{ij}^{gg} / d\delta z$ varies from -4 to 4 and behaves distinctively different from one pair of i and j to another (figure 1).

4.3. Joint analysis of BAO and WL

Based on figure 3 and figure 4, one expects a great improvement of errors on cosmological parameters when BAO and WL are analysed jointly, which is indeed demonstrated in figure 5. The combination (shaded area) reduces the EP by more than a factor of 6 compared to that of LSST WL alone (solid line). This is more than the factor of $\sim \sqrt{2}$ reported in [33], which does not include systematic errors or uncertainties in the photo- z error distribution. LSST BAO (dotted line) does not seem competitive to WL at all, if assessed by $\sigma(w_0)$ and $\sigma(w_a)$ only. Since the errors in $\sigma(w_0)$ and $\sigma(w_a)$ are highly correlated, the EP of BAO is merely a factor of 1.47 larger than that of WL (see figure 6 and table 3). The important issue here is not that which technique is better, but rather that one must analyse BAO and WL data (and possibly others) *jointly* to overcome the weakness of each.

To understand the role of the growth function, we artificially fix the galaxy clustering bias parameters for BAO, which enables BAO to utilise the growth information. Since the growth function and galaxy bias are degenerate, the error of the growth function, if similarly parametrized, is the same as that of the galaxy bias. However, when the galaxy bias is fixed, the error of the growth function will be much smaller than that of the galaxy bias in figure 4. The resulting constraints

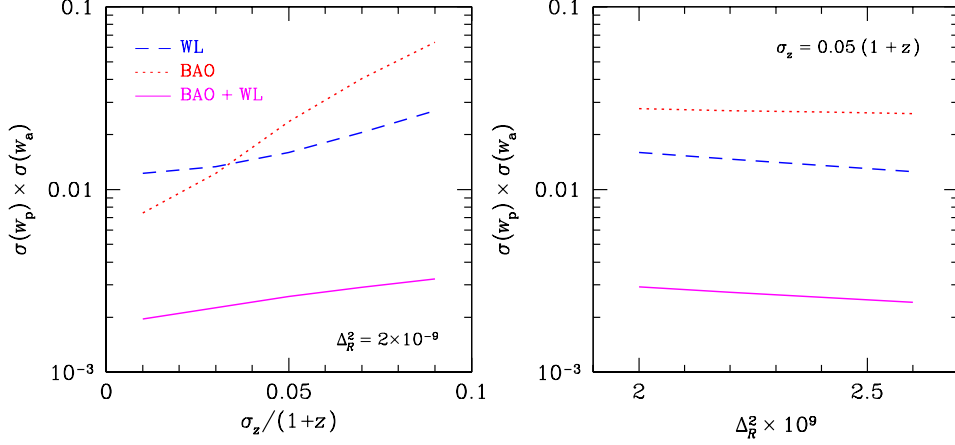


Figure 6. *Left panel:* The EP as a function of the rms photo- z error σ_z for LSST BAO (dotted line), LSST WL (dashed line), and the two combined (solid line). We have applied the same tomographic binning regardless of the value of σ_z . With finer bins, BAO results can be further improved at small σ_z , although WL and the combined results will remain less sensitive to σ_z . *Right panel:* The EP as a function of the normalisation of the primordial curvature fluctuation Δ_R^2 at $k = 0.05 \text{ Mpc}^{-1}$. As Δ_R^2 increases, the galaxy number density fluctuation and weak lensing shear signal increase. If the signal is dominant over the noise (in a single mode), then the constraints on w_0 and w_a will not change with the normalisation, whereas in the opposite case $\sigma(w_0)$ and $\sigma(w_a)$ will be inversely proportional to the normalisation. To isolate the effect of the normalisation, we use the same maximum multipole of BAO, which is determined for $\Delta_R^2 = 2.6 \times 10^{-9}$, for all normalisation cases. This means that the constraints with $\Delta_R^2 < 2.6 \times 10^{-9}$ are calculated from fewer multipoles than what would otherwise be included with the criteria $\Delta_\delta^2(k; z) < 0.4$ and $40 \leq \ell \leq 3000$.

(dashed line in figure 5) on w_0 and w_a are, not surprisingly, as tight as those of BAO and WL combined, because the narrow kernel of BAO makes it possible to sample the cosmic density field at very fine intervals in redshift [see also 21]. We note, however, that the determination of the (product of the galaxy clustering bias and) growth and distance are correlated. If the distance is poorly measured, the growth is not likely to be known very well either. Conversely, an accurate determination of the growth can improve the distance measurements, because the amplitude of the BAO and WL power spectra depend on the distance (not just distance ratios).

Error forecasts inevitably depend on the assumed fiducial model. For example, because of its narrow kernel, BAO is sensitive to the rms photo- z error σ_z , which can vary greatly with the galaxy population, filter design, survey depth, and so on. Another parameter of interest is the normalisation of the matter power spectrum, which is proportional to the normalisation Δ_R^2 of the primordial curvature power spectrum at $k = 0.05 \text{ Mpc}^{-1}$. Accompanying a lower estimate of the electron optical depth to the last scattering surface $\tau = 0.09$ and a slight tilt $n_s = 0.951$, the recent analysis of the three-year *WMAP* data lowers the value of Δ_R^2 by 25%. This reduces the amplitude of BAO and WL power spectra and can result in a weakening of the parameter constraints by up to 25% if the shot (shape) noise and systematic noise are dominant over the (auto power spectra) signal in a single mode.

Figure 6 quantifies the dependence of the EP on σ_z (left panel) and Δ_R^2 , (right

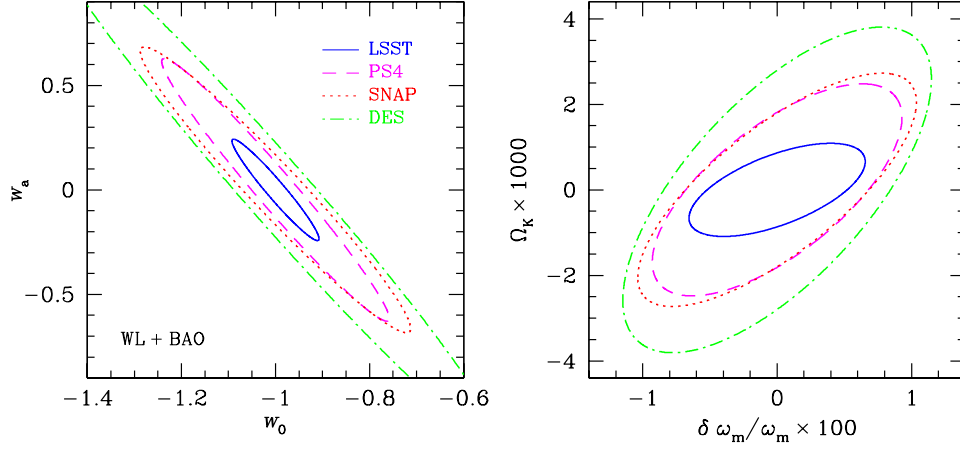


Figure 7. *Left panel:* Joint BAO and WL constraints on the dark energy EOS parameters w_0 and w_a for DES (dash-dotted line), LSST (solid line), PS4 (dashed line), and SNAP (dotted line). *Right Panel:* Same as the left panel, but for the matter density ω_m and curvature term Ω_K . Note that *Planck* alone constrains ω_m to $\sim 1\%$ (see table 3) and that SN and cluster counting can further improve the constraints.

panel). The sensitivity of BAO (dotted line) and, to a lesser degree, WL (dashed line) EPs to σ_z is clearly seen, and the combination (solid line) is less sensitive to σ_z . From the right panel, one sees that the BAO EP does not change much with the normalisation Δ_R^2 . This means that it is not limited by noise, but rather by the photo- z error: with 40 bins whose widths are proportional to $(1 + z_p)$, the bins are already narrower than the photo- z rms. The WL EP improves by 28%, i.e., roughly 14% each on w_p and w_a , as the normalisation increases from $\Delta_R^2 = 2 \times 10^{-9}$ to 2.6×10^{-9} , indicating that the noise is more important for WL but not yet completely dominant.

4.4. Forecasts

We present w_0 - w_a and ω_m - Ω_K 1σ error contours of joint BAO and WL analysis for the four surveys in figure 7 and list the 1σ error bounds on all the cosmological parameters in table 3 (optimistic case) and table 4 (pessimistic case).

Figure 7 demonstrates that a deep and wide survey like LSST can tighten the constraints on dark energy and other cosmological parameters substantially. In its wide and shallow survey mode, PS4 can perform equally well as SNAP. Of course, the SNAP SN program will provide additional constraints that are fairly complementary to BAO and WL [e.g., 21]. Likewise, the three ground-based surveys all plan to carry out SN and/or cluster counting to some degree.

With $w = -1$, the combination of *WMAP* and the Supernova Legacy Survey data determines Ω_K at a few percent level [9]. The right panel of figure 7 shows that LSST BAO+WL and *Planck* can further reduce the uncertainty to 10^{-3} with our parametrization of the dark energy EOS, which may lead to interesting tests of inflation [21, 111]. It is also possible to measure the mean curvature from BAO and WL without assuming the dynamics and content of the universe [39]. Though less constraining, such a model independent method can provide a very useful check.

Our forecasts for *Planck* are given in table 3 for reference. CMB is affected by

Table 3. Error forecasts with optimistic BAO and WL survey parameters

Survey	BAO	WL	w_p^a	w_0^b	w_a^b	$\ln \omega_m$	$\ln \omega_b$	θ_s	Ω_K	τ^c	Y_p	n_s	α^d	$\ln \Delta_R^{2c}$
						(10^{-3})								
<i>Planck</i>			0.47	1.1	2.5	9.5	11	0.19	17	9.4	16	9.8	8.1	19
LSST	×		0.037	0.26	0.64	5.1	6.5	0.14	1.1	8.9	7.0	4.2	0.81	18
		×	0.044	0.16	0.36	8.5	8.9	0.16	2.5	8.8	10	6.5	0.73	18
	×	×	0.016	0.061	0.16	4.3	5.8	0.13	0.72	6.1	5.4	2.7	0.41	12
PS4	×		0.075	0.49	1.3	6.8	8.5	0.16	3.1	9.0	11	6.8	2.1	18
		×	0.083	0.52	1.2	8.8	9.2	0.16	3.3	9.1	11	7.2	1.8	18
	×	×	0.034	0.16	0.41	6.1	7.4	0.14	1.6	8.1	8.3	5.0	1.3	16
SNAP	×		0.12	0.84	2.1	7.7	8.8	0.16	3.4	9.0	11	7.1	2.2	18
		×	0.11	0.44	0.86	8.8	9.2	0.16	2.9	9.1	11	7.2	1.8	18
	×	×	0.046	0.19	0.45	6.8	7.6	0.15	1.8	8.4	8.2	5.0	1.2	16
DES	×		0.14	0.90	2.4	8.0	9.1	0.17	5.5	9.0	12	7.8	3.6	18
		×	0.16	1.0	2.4	8.8	9.3	0.17	4.6	9.2	12	7.6	3.2	18
	×	×	0.058	0.31	0.80	7.6	8.4	0.15	2.5	8.7	10	6.4	2.3	17

^a The error of the dark energy EOS at the pivot epoch [equation (15)], $\sigma(w_p)$, is uncorrelated with that of w_a .

^b When combining CMB with BAO and WL, we do not include the CMB constraints on w_0 and w_a , which are sensitive to the late-time ISW effect on large scales [112].

^c If the polarisation data at $2 \leq \ell < 10$ are included, *Planck* alone can achieve $\sigma(\tau) = 0.0049$ and $\sigma(\ln \Delta_R^2) = 0.010$.

^d The running $\alpha = d \ln n_s(k) / d \ln k$ at $k_f = 0.05 \text{ Mpc}^{-1}$, and the primordial curvature power spectrum $\Delta_R^2(k) = \Delta_R^2(k_f)(k/k_f)^{n_s(k_f)-1+0.5\alpha \ln(k/k_f)}$ is accurate to second order.

^e Without the self-calibration of photo- z parameters from the galaxy cross power spectra, the dark energy constraints would degrade to $\sigma(w_p) = 0.021$, $\sigma(w_0) = 0.094$, and $\sigma(w_a) = 0.22$. One could achieve $\sigma(w_p) = 0.012$, $\sigma(w_0) = 0.048$, and $\sigma(w_a) = 0.13$, if $N_{\text{sys}}^g = N_{\text{sys}}^\gamma = 0$.

Table 4. Error forecasts with pessimistic BAO and WL survey parameters

Survey	BAO	WL	w_p	w_0	w_a	$\ln \omega_m$	$\ln \omega_b$	θ_s	Ω_K	τ	Y_p	n_s	α	$\ln \Delta_R^2$
						(10^{-3})								
LSST	×		0.039	0.28	0.69	5.2	6.7	0.14	1.2	9.0	7.3	4.4	0.90	18
		×	0.067	0.28	0.57	8.6	8.9	0.16	2.6	8.9	10	6.6	0.74	18
	×	×	0.019	0.069	0.18	4.4	5.9	0.13	0.78	6.3	5.6	2.9	0.44	12
PS4	×		0.078	0.52	1.4	7.0	8.6	0.16	3.3	9.1	11	7.0	2.5	18
		×	0.13	0.90	2.0	8.8	9.2	0.16	3.7	9.1	11	7.3	2.0	18
	×	×	0.037	0.18	0.46	6.3	7.6	0.15	1.8	8.2	8.6	5.2	1.5	16
SNAP	×		0.13	0.92	2.2	7.8	8.9	0.16	3.6	9.1	1.1	7.2	2.4	18
		×	0.14	0.53	1.0	8.8	9.2	0.16	3.0	9.1	11	7.2	1.8	18
	×	×	0.057	0.23	0.52	7.0	7.7	0.15	1.9	8.5	8.4	5.2	1.3	17
DES	×		0.15	0.99	2.6	8.1	9.2	0.17	6.1	9.1	13	8.0	4.1	18
		×	0.22	1.4	3.2	8.8	9.3	0.17	5.3	9.2	12	7.7	3.4	18
	×	×	0.065	0.35	0.90	7.7	8.6	0.16	2.7	8.8	11	6.6	2.7	18

dark energy mostly through the late-time ISW effect on large angular scales [112]. If we limit the multipoles to $\ell \geq 40$ for *Planck*, then its EP increases to 11. Since the properties of the cosmic density field on very large scales have not been measured very well yet, we neglect *Planck* constraints on the dark energy EOS parameters when combining it with BAO and WL. This treatment does not affect the combined results, especially those of all the three techniques, because w_0 and w_a are better measured by BAO and WL. For non-dark-energy parameters (excluding Ω_K and α), the constraints are not so easily improved by BAO and WL except for LSST, which shows again that the deep photometry and wide area are not merely a technical challenge but rather a requirement for BAO and WL to be competitive with future CMB measurements beyond the dark energy EOS [110].

As a result of its fine sampling of the density field in redshift space, BAO does relatively well in measuring parameters (ω_m and ω_b) that affect the features in the power spectrum. Since noises are more dominant for WL (see figure 3 and figure 6), BAO can perform better than WL for shallow surveys, especially in the pessimistic case (table 4). BAO has another slight advantage that it probes the universe at a little higher redshift than WL does, because the lensing kernel peaks below the redshift of source galaxies. This advantage fades away when the survey is shallow and/or narrow, and it is a part of the reason that the relative strength of the BAO and WL constraints on Ω_K inverts from LSST to DES. For SNAP, its high galaxy number density (low shape noise) allows WL to remain significantly more competitive than BAO in the pessimistic case.

Our errors of the running α for LSST WL and SNAP WL are considerably tighter than those in [19], but the errors for DES BAO are larger than those forecasted for a $f_{\text{sky}} = 0.1$ and $z < 2.3$ BAO survey in [40]. Since we do not include neutrino mass as [19] does, and since [40] assumes a survey with many more galaxies than DES, our results can still be consistent with theirs. Despite the differences, these forecasts all predict fairly tight constraints on α , which is expected to be of the same order as $(n_s - 1)^2$ from simple inflation models. With $n_s - 1 = 0.05$ [9] and measurements of α at 10^{-3} level from future BAO and WL surveys, we will have another interesting test for inflation [19].

Comparing the optimistic forecasts with pessimistic ones, we find that the joint BAO and WL results are fairly robust to the priors on non-cosmological parameters and to simple additive systematics. This clearly demonstrates the necessity of utilising multiple techniques jointly to extract cosmology information.

5. Discussion and Conclusions

We have shown that BAO and WL are highly complementary to each other especially in the presence of the uncertainties of the photo- z error distribution and inaccurate knowledge of the galaxy clustering bias. For non-Gaussian photo- z errors, more parameters will be needed to characterise the error distribution, which inevitably leads to weaker constraints on these parameters [86]. The impact of non-Gaussian photo- z errors on the forecasts of cosmological parameters will be investigated separately.

We emphasise that one cannot rely solely on the galaxy power spectra for photo- z information. One may notice in figure 4 that the galaxy clustering bias and photo- z parameters are not constrained by the galaxy power spectra at both the low-redshift end, where very few power spectrum modes can be used, and the high-redshift end, where the data are poor. With long-tail photo- z error models, the unconstrained

errors at the two redshift ends can easily propagate to the whole redshift range and diminish the BAO ability to self-calibrate the photo- z parameters. In order to achieve the BAO self-calibration of photo- z errors, one must know how to parametrize the probability distribution of photo- z errors faithfully. In other words, it is crucial to map the photo- z error distribution and reduce its uncertainties as much as possible with massive spectroscopic calibrations *and* state-of-the-art photo- z algorithms.

Even without knowing the true photo- z error distribution accurately, one can still use the tomographic BAO and WL power spectra to check for deviations from the assumed photo- z error distribution and to detect certain systematic errors. For example, a detection of the cross power spectrum between a very low redshift BAO bin and a high redshift one above the expected level could be a result of catastrophic photo- z errors between the bins or residuals of extinction correction. The effect of the former would be confined between the bins around the two redshifts, while that of the latter would be likely to spread over all bins. In any case, the cross power spectra arising from the two causes would have distinct shapes. Similarly, an unexpected detection of the cross power spectrum between a low redshift WL bin and a higher redshift BAO bin could be due to some systematics.

We have assumed that the galaxy bias is not correlated with photo- z errors. In reality, different types of galaxies have different spectral features that affect their photo- z estimation and, meanwhile, do not cluster with the same strength. Therefore, photo- z errors are inevitably coupled with the galaxy bias through the galaxy type. More realistic forecasts should include multiple types of galaxies and assign separate galaxy bias and photo- z parameters for each type. Since the shot noise is relatively low for BAO, it is practical to split the galaxies into a few groups for better analyses. One may actually improve the photo- z constraints with multiple galaxy types [86].

One may worry about the break-down of the Limber approximation on large angular scales. The break-down of an approximation is not a loss of information, but, rather, a demand for proper means to extract the information. For parameter estimation, full calculations should replace the Limber approximation on large angular scales, but for error estimation, we can make more conservative cuts in ℓ to see the effect of completely ignoring the large-scale information. If we set the minimum multipole to $\ell_{\min} = 100$, which removes the information of the broadband shape of the matter power spectrum (see figure 1), the constraints on w_0 and w_a degrade by less than 20% for LSST BAO and less than 13% for the joint analysis. In this test, BAO bins below $z_p = 0.23$ have no multipole usable. BAO errors on w_0 and w_a will double if one also excludes the first few acoustic peaks by setting $\ell_{\min} = 300$. In contrast, WL errors will only increase by 25% with $\ell_{\min} = 300$. These tests confirm that the constraining power of the broadband shape of the matter power spectrum is sub-dominant to that of the acoustic oscillations for the BAO technique [32].

On the other end of the scales, one may worry about our somewhat aggressive maximum multipoles $\ell_{\max} = 3000$ for BAO and $\ell_{\max} = 2000$ for WL. We find that a cut of $\ell_{\max} = 2000$ for LSST BAO increases the error on w_0 and w_a by less than 2%. This is not surprising, because the angular galaxy power spectra of the 15 ($z_p > 1.7$) BAO bins that are affected by this cut are practically featureless at $2000 < \ell \leq 3000$, i.e., these multipoles do not contribute much to distance measurements. With $\ell_{\max} = 2000$ for BAO and $\ell_{\max} = 1000$ for WL, the LSST BAO and WL joint constraints on w_0 and w_a weaken by only 8%. Hence, we conclude that, given the survey parameters and assumptions about systematics, our forecasts are fairly robust against the range of multipoles included in the analysis.

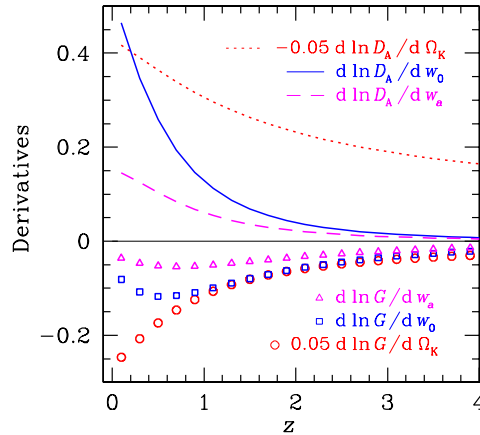


Figure 8. Derivatives of the comoving angular diameter distance D_A and linear growth function G with respect to w_0 , w_a , and Ω_K . When taking the derivatives, we hold the angular size of the sound horizon at the last scattering surface θ_s fixed. At $z \sim 0$, the distance derivatives are effectively derivatives of the implicit Hubble constant with respect to the parameters. The linear growth function is normalised such that $G(a) = a$ in an Einstein-de Sitter universe [as opposed to $G(1) = 1$ regardless the cosmological model].

There have been interesting discussions about dark energy constraints from measurements of the distance and the growth of the large-scale structure. The results, depending on how the distance and growth are separated, range from that they are equally powerful [64, 66] to that the constraints from the growth function are much weaker than those from the distance [20, 62]. The relative strength of the distance and growth function in constraining dark energy depends on how sensitive the distance and growth function are to the parameters and how well they can be reconstructed from WL data.

We plot the distance and growth derivatives with respect to w_0 , w_a , and Ω_K in figure 8. Since the growth function (open symbols) is less sensitive to the parameters than the distance (lines) and it is not so well determined as the distance with WL [20], dark energy constraints from the growth are sub-dominant to those from the distance. However, this should not undermine the advantage of being able to measure the growth function (or, more appropriately, the amplitude of the matter power spectrum). To measure the distance with WL, one needs to know how the power spectrum amplitude changes with redshift, because the shear power spectrum depends on both the lensing geometry and growth function. In fact, the WL EP will increase by more than 10 times, if one gives up the ability to measure the growth function by applying artificial bias parameters [with the fiducial value $b = 1$ and $\sigma_P(\ln b) = 0.2$] to the shear power spectra [21]. Conversely, it is not possible to measure the growth function accurately if the distance is not, because one needs to know the scale $k = \ell/D_A$ accurately to estimate the amplitude of the power spectrum.

The galaxy power spectra, being able to use the BAO features in the matter power spectrum, can better isolate the distance from (the product of the galaxy bias and) growth [44], which partially explains the $\lesssim 10\%$ difference in the BAO constraints between the optimistic case [table 3 with $\sigma_P(\ln b) = 0.15$] and pessimistic case [table 4 with $\sigma_P(\ln b) = 0.3$]. On the other hand, if the galaxy bias was known perfectly, then

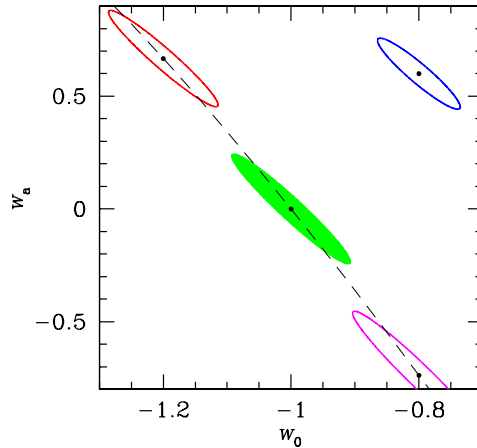


Figure 9. Error contours in the w_0 - w_a plane with joint LSST BAO and WL analysis. Solid dots mark the fiducial values of w_0 and w_a . All the four models have the same fiducial values of the other 9 cosmological parameters. The effects of w_0 and w_a on the angular size of the sound horizon at the last scattering surface θ_s cancel each other along the thin dashed line. In other words, we require that the two implicit parameters Ω_X and h be the same for models on this line. The supergravity-inspired model at $(w_0, w_a) = (-0.8, 0.6)$ has $\Omega_X = 0.61$ and $h = 0.57$.

one could determine the distance with both the amplitude and BAOs of the galaxy power spectra. This reduces errors in both the distance and growth function and leads to the tight dark energy constraints of the BAO+G case in figure 5.

Figure 8 also illustrates why SN constraints on dark energy are sensitive to the flatness assumption [21, 113]. The reason is that distance is much more sensitive to curvature than to the dark energy EOS. In addition, the (negative) distance derivative with respect to Ω_K (dotted line) has a redshift dependence that somewhat resembles $d \ln D_A / dw_a$ (dashed line), so that a small freedom in Ω_K at the percent level can greatly degrade the constraint on w_a . Similarly, the relatively tighter constraint on w_0 compared to that on w_a with all techniques can be explained by the relative amplitude of the derivatives. Since the distance derivative $d \ln D_A / d\Omega_K$ decreases more slowly with increasing redshift than $d \ln D_A / dw_0$ (solid line) and $d \ln D_A / dw_a$, the degeneracy between dark energy and curvature can be lifted by extending the measurements to higher redshift. This explains the factor of ~ 3 difference in BAO $\sigma(\Omega_K)$ between the LSST survey and the shallower PS4 survey. The magnitude of the growth derivative with respect to Ω_K (open circles) is at least 20 times larger than those with respect to w_0 (open squares) and w_a (open triangles); the relative sign between the growth and distance derivatives with respect to Ω_K is opposite to those with respect to w_0 and w_a . Consequently, WL, being able to measure the growth function, can determine the curvature well even without high-redshift data, so that the PS4 WL constraint on Ω_K is only moderately worse than that of LSST.

Finally, we present the joint constraints of LSST BAO and WL for some interesting dark energy models in figure 9. All the models assume the same fiducial values for the other 9 cosmological parameters, i.e., essentially, the same distance to the last scattering surface. This requires modifications to the two implicit parameters: $\Omega_X = 0.61$ and $h = 0.57$ for the supergravity-inspired model at $(w_0, w_a) = (-0.8, 0.6)$.

For the models along the dashed line, $\Omega_X = 0.76$ and $h = 0.73$ are preserved as well. In other words, w_0 and w_a are degenerate along the dashed line, if the distance to the last scattering surface is the only constraint on dark energy. Figure 9 demonstrates that a joint analysis of LSST BAO and WL can indeed distinguish between some dark energy models that are quite degenerate to CMB or WL alone. Therefore, it is promising that, with multiple techniques as well as various statistics of the same galaxy and shear data, we will gain valuable insight to the mystery of dark energy from ambitious multiband imaging surveys.

Acknowledgments

We thank Gary Bernstein for many helpful comments, and Sarah Bridle, Lloyd Knox, Michael Schneider, Yong-Seon Song, Anthony Tyson, and David Wittman for useful conversations and suggestions. This work was supported by NSF under Grant No. 0307961 and 0441072 and NASA under grant No. NAG5-11098.

Appendix A. Linear growth function

Assuming that dark energy is spatially homogeneous, we can solve the the linear growth function $G(a)$ from the linear perturbation equation

$$G''(a) + \frac{G'(a)}{2a} \{4 - \Omega_m(a) - \Omega_X(a) [1 + 3w(a)]\} = \frac{3\Omega_m(a)}{2a^2} G(a), \quad (\text{A.1})$$

where $\Omega_X(a)$ is the ratio of dark energy density to the critical density, and

$$\begin{aligned} \Omega_m(a) &= a^{-3} E^{-2}(a) \Omega_m, \\ \Omega_X(a) &= E^{-2}(a) \Omega_X \exp \left\{ 3 \int_a^1 d \ln a' [1 + w(a')] \right\}, \\ E^2(a) &= H_0^{-2} H^2(a) = a^{-3} \Omega_m + a^{-2} (1 - \Omega_m - \Omega_X) + \\ &\quad \Omega_X \exp \left\{ 3 \int_a^1 d \ln a' [1 + w(a')] \right\}, \end{aligned}$$

with $\Omega_m \equiv \Omega_m(1)$ and $\Omega_X \equiv \Omega_X(1)$. For a flat universe, (A.1) reduces to the form in [114]. With a matter-dominated universe at $a \ll 1$, we set the initial condition to $G(a_i) = a_i$, where the starting expansion factor satisfies $|G''(a_i)| \ll 1$. The radiation component is dropped in the initial condition to follow the convention $G(a) = a$ in an Einstein-de Sitter universe. This is appropriate since we are only concerned with the relative growth in matter era. The linear growth function may be normalised so that $G(1) = 1$ regardless the cosmological model in some applications.

Appendix B. Nonlinear matter power spectrum

Fitting formulae that are calibrated with N -body simulations [96, 115] are widely used to map the linear matter power spectrum to nonlinear matter power spectrum. We use the PD96 formula [96] for convenience. However, modifications are necessary for the following reasons: (1) PD96 formula expects the logarithmic slope of the linear power spectrum to be monotonic, which is not satisfied with BAOs, and (2) it maps the linear wavenumber to nonlinear wavenumber, which would shift the scales of BAOs dramatically. To overcome these problems, we use a smooth fitting formula

[116] of the linear power spectrum without BAOs, $\Delta_{\text{NB,L}}^2(k)$, that otherwise matches the power spectrum with BAOs, $\Delta_{\text{BAO,L}}^2(k)$, to calculate the nonlinear matter power spectrum, $\Delta_{\text{NB}}^2(k)$. The final nonlinear matter power spectrum with BAOs is then $\Delta_{\text{BAO}}^2(k) = \Delta_{\text{BAO,L}}^2(k)\Delta_{\text{NB}}^2(k)/\Delta_{\text{NB,L}}^2(k)$. We also note that one may use third-order perturbation theory to calculate the nonlinear matter power spectrum with BAOs at $z > 1$ [117], but there is no clear demonstration that the large error of the perturbative calculations at lower redshift [118] has been rectified.

References

- [1] Riess A G *et al.*, 1998 *Astron. J.* **116** 1009–1038
- [2] Perlmutter S *et al.*, 1999 *Astrophys. J.* **517** 565–586
- [3] Tonry J L *et al.*, 2003 *Astrophys. J.* **594** 1–24
- [4] Riess A G *et al.*, 2004 *Astrophys. J.* **607** 665–687
- [5] Dodelson S and Knox L, 2000 *Physical Review Letters* **84** 3523–3526
- [6] Percival W J *et al.*, 2002 *Mon. Not. Roy. Astron. Soc.* **337** 1068–1080
- [7] Spergel D N *et al.*, 2003 *Astrophys. J. Supp.* **148** 175–194
- [8] Tegmark M *et al.*, 2004 *Phys. Rev. D* **69**(10) 103501–+
- [9] Spergel D N *et al.*, 2006 *Preprint astro-ph/0603449*
- [10] Peebles P J E and Yu J T, 1970 *Astrophys. J.* **162** 815–+
- [11] Bond J R and Efstathiou G, 1984 *Astrophys. J. Lett.* **285** L45–L48
- [12] Holtzman J A, 1989 *Astrophys. J. Supp.* **71** 1–24
- [13] Hu W and Tegmark M, 1999 *Astrophys. J. Lett.* **514** L65–L68
- [14] Hu W, 2002 *Phys. Rev. D* **66**(8) 083515–+
- [15] Huterer D, 2002 *Phys. Rev. D* **65**(6) 063001–+
- [16] Refregier A, 2003 *Ann. Rev. Astron. & Astrophys.* **41** 645–668
- [17] Ishak M, Hirata C M, McDonald P and Seljak U, 2004 *Phys. Rev. D* **69**(8) 083514–+
- [18] Takada M and Jain B, 2004 *Mon. Not. Roy. Astron. Soc.* **348** 897–915
- [19] Song Y S and Knox L, 2004 *Phys. Rev. D* **70**(6) 063510–+
- [20] Knox L, Song Y S and Tyson J A, 2006 *Phys. Rev. D* **74**(2) 023512–+
- [21] Knox L, Song Y S and Zhan H, 2006 *Preprint astro-ph/0605536*
- [22] Haiman Z, Mohr J J and Holder G P, 2001 *Astrophys. J.* **553** 545–561
- [23] Hu W, 2003 *Phys. Rev. D* **67**(8) 081304–+
- [24] Lima M and Hu W, 2004 *Phys. Rev. D* **70**(4) 043504–+
- [25] Lima M and Hu W, 2005 *Phys. Rev. D* **72**(4) 043006–+
- [26] Eisenstein D J, Hu W and Tegmark M, 1998 *Astrophys. J. Lett.* **504** L57
- [27] Cooray A, Hu W, Huterer D and Joffre M, 2001 *Astrophys. J. Lett.* **557** L7–L10
- [28] Bartelmann M and Schneider P, 2001 *Phys. Rep.* **340** 291–472
- [29] Blake C and Glazebrook K, 2003 *Astrophys. J.* **594** 665–673
- [30] Hu W and Haiman Z, 2003 *Phys. Rev. D* **68**(6) 063004–+

- [31] Linder E V, 2003 *Phys. Rev. D* **68**(8) 083504–+
- [32] Seo H and Eisenstein D J, 2003 *Astrophys. J.* **598** 720–740
- [33] Hu W and Jain B, 2004 *Phys. Rev. D* **70**(4) 043009–+
- [34] Angulo R, Baugh C M, Frenk C S, Bower R G, Jenkins A and Morris S L, 2005 *Mon. Not. Roy. Astron. Soc.* **362** L25–L29
- [35] Blake C and Bridle S, 2005 *Mon. Not. Roy. Astron. Soc.* **363** 1329–1348
- [36] Glazebrook K and Blake C, 2005 *Astrophys. J.* **631** 1–20
- [37] Seo H J and Eisenstein D J, 2005 *Astrophys. J.* **633** 575–588
- [38] White M, 2005 *Astroparticle Physics* **24** 334–344
- [39] Bernstein G, 2006 *Astrophys. J.* **637** 598–607
- [40] Dolney D, Jain B and Takada M, 2006 *Mon. Not. Roy. Astron. Soc.* **366** 884–898
- [41] Eisenstein D J, Seo H J and White M, 2006 *Preprint astro-ph/0604361*
- [42] Eisenstein D J, Seo H J, Sirko E and Spergel D, 2006 *Preprint astro-ph/0604362*
- [43] Wang Y, 2006 *Astrophys. J.* **647** 1–7
- [44] Zhan H and Knox L, 2006 *Astrophys. J.* **644** 663–670
- [45] Chevallier M and Polarski D, 2001 *International Journal of Modern Physics D* **10** 213–223
- [46] Bernstein G and Jain B, 2004 *Astrophys. J.* **600** 17–25
- [47] Ishak M and Hirata C M, 2005 *Phys. Rev. D* **71**(2) 023002–+
- [48] Ma Z, Hu W and Huterer D, 2006 *Astrophys. J.* **636** 21–29
- [49] Huterer D, Takada M, Bernstein G and Jain B, 2006 *Mon. Not. Roy. Astron. Soc.* **366** 101–114
- [50] White M, 2004 *Astroparticle Physics* **22** 211–217
- [51] Zhan H and Knox L, 2004 *Astrophys. J. Lett.* **616** L75–L78
- [52] Hagan B, Ma C P and Kravtsov A V, 2005 *Astrophys. J.* **633** 537–541
- [53] Heitmann K, Ricker P M, Warren M S and Habib S, 2005 *Astrophys. J. Supp.* **160** 28–58
- [54] Zhan H, 2006 *Astrophys. J.* **639** 617–620
- [55] Huterer D and Takada M, 2005 *Astroparticle Physics* **23** 369–376
- [56] Ratra B and Peebles P J E, 1988 *Phys. Rev. D* **37** 3406–3427
- [57] Huey G, Wang L, Dave R, Caldwell R R and Steinhardt P J, 1999 *Phys. Rev. D* **59**(6) 063005–+
- [58] Perlmutter S, Turner M S and White M, 1999 *Physical Review Letters* **83** 670–673
- [59] Wang L, Caldwell R R, Ostriker J P and Steinhardt P J, 2000 *Astrophys. J.* **530** 17–35
- [60] Dvali G, Gabadadze G and Porrati M, 2000 *Physics Letters B* **485** 208–214
- [61] Deffayet C, 2001 *Physics Letters B* **502** 199–208
- [62] Abazajian K and Dodelson S, 2003 *Physical Review Letters* **91**(4) 041301–+
- [63] Linder E V, 2004 *Phys. Rev. D* **70**(2) 023511–+

- [64] Simpson F and Bridle S, 2005 *Phys. Rev. D* **71**(8) 083501–+
- [65] Song Y S, 2005 *Phys. Rev. D* **71**(2) 024026–+
- [66] Zhang J, Hui L and Stebbins A, 2005 *Astrophys. J.* **635** 806–820
- [67] Bacon D J, Refregier A R and Ellis R S, 2000 *Mon. Not. Roy. Astron. Soc.* **318** 625–640
- [68] Wittman D M, Tyson J A, Kirkman D, Dell’Antonio I and Bernstein G, 2000 *Nature* **405** 143–148
- [69] Van Waerbeke L *et al.*, 2001 *Astron. & Astrophys.* **374** 757–769
- [70] Jarvis M, Bernstein G M, Fischer P, Smith D, Jain B, Tyson J A and Wittman D, 2003 *Astron. J.* **125** 1014–1032
- [71] Hoekstra H, Mellier Y, van Waerbeke L, Semboloni E, Fu L, Hudson M J, Parker L C, Tereno I and Benabed K, 2006 *Astrophys. J.* **647** 116–127
- [72] Eisenstein D J *et al.*, 2005 *Astrophys. J.* **633** 560–574
- [73] Cole S *et al.*, 2005 *Mon. Not. Roy. Astron. Soc.* **362** 505–534
- [74] Hütsi G, 2006 *Astron. & Astrophys.* **449** 891–902
- [75] Ilbert O *et al.*, 2006 *Preprint astro-ph/0603217*
- [76] Padmanabhan N *et al.*, 2005 *Mon. Not. Roy. Astron. Soc.* **359** 237–250
- [77] Padmanabhan N *et al.*, 2006 *Preprint astro-ph/0605302*
- [78] Blake C, Collister A, Bridle S and Lahav O, 2006 *Preprint astro-ph/0605303*
- [79] Schneider P, 1998 *Astrophys. J.* **498** 43–+
- [80] Yee H K C, 1998 *Preprint astro-ph/9809347*
- [81] Connolly A J, Szalay A S, Dickinson M, Subbarao M U and Brunner R J, 1997 *Astrophys. J. Lett.* **486** L11+
- [82] Benítez N, 2000 *Astrophys. J.* **536** 571–583
- [83] Fontana A, D’Odorico S, Poli F, Giallongo E, Arnouts S, Cristiani S, Moorwood A and Saracco P, 2000 *Astron. J.* **120** 2206–2219
- [84] Babbedge T S R, Rowan-Robinson M, Gonzalez-Solares E, Polletta M, Berta S, Pérez-Fournon I, Oliver S, Salaman D M, Irwin M and Weatherley S J, 2004 *Mon. Not. Roy. Astron. Soc.* **353** 654–672
- [85] Mobasher B *et al.*, 2004 *Astrophys. J. Lett.* **600** L167–L170
- [86] Schneider M, Knox L, Zhan H and Connolly A, 2006 *Preprint astro-ph/0606098*
- [87] Newman J, 2006 In preparation
- [88] Limber D N, 1954 *Astrophys. J.* **119** 655–+
- [89] Kaiser N, 1992 *Astrophys. J.* **388** 272–286
- [90] Verde L *et al.*, 2002 *Mon. Not. Roy. Astron. Soc.* **335** 432–440
- [91] Tegmark M *et al.*, 2004 *Astrophys. J.* **606** 702–740
- [92] Tegmark M *et al.*, 2002 *Astrophys. J.* **571** 191–205
- [93] Guzik J and Bernstein G, 2005 *Phys. Rev. D* **72**(4) 043503–+
- [94] Jain B, Jarvis M and Bernstein G, 2006 *Journal of Cosmology and Astro-Particle Physics* JCAP02(2006)001

- [95] Zaldarriaga M and Seljak U, 2000 *Astrophys. J. Supp.* **129** 431–434
- [96] Peacock J A and Dodds S J, 1996 *Mon. Not. Roy. Astron. Soc.* **280** L19–L26
- [97] Zaldarriaga M, Spergel D N and Seljak U, 1997 *Astrophys. J.* **488** 1–+
- [98] Eisenstein D J, Hu W and Tegmark M, 1999 *Astrophys. J.* **518** 2–23
- [99] Kaplinghat M, Knox L and Song Y S, 2003 *Physical Review Letters* **91**(24) 241301–+
- [100] Sachs R K and Wolfe A M, 1967 *Astrophys. J.* **147** 73–+
- [101] Jungman G, Kamionkowski M, Kosowsky A and Spergel D N, 1996 *Phys. Rev. D* **54** 1332–1344
- [102] Vogeley M S and Szalay A S, 1996 *Astrophys. J.* **465** 34–+
- [103] Tegmark M, Taylor A N and Heavens A F, 1997 *Astrophys. J.* **480** 22–+
- [104] Tegmark M, 1997 *Physical Review Letters* **79** 3806–3809
- [105] Cooray A and Hu W, 2001 *Astrophys. J.* **554** 56–66
- [106] Weinberg D H, Davé R, Katz N and Hernquist L, 2004 *Astrophys. J.* **601** 1–21
- [107] Hoekstra H, van Waerbeke L, Gladders M D, Mellier Y and Yee H K C, 2002 *Astrophys. J.* **577** 604–614
- [108] Seljak U, Makarov A, Mandelbaum R, Hirata C M, Padmanabhan N, McDonald P, Blanton M R, Tegmark M, Bahcall N A and Brinkmann J, 2005 *Phys. Rev. D* **71**(4) 043511–+
- [109] Martin D and Albrecht A, 2006 *Preprint astro-ph/0604401*
- [110] Zhan H, Knox L, Tyson J A and Margoniner V, 2006 *Astrophys. J.* **640** 8–17
- [111] Knox L, 2006 *Phys. Rev. D* **73**(2) 023503–+
- [112] Hu W, 2002 *Phys. Rev. D* **65**(2) 023003–+
- [113] Linder E V, 2005 *Astroparticle Physics* **24** 391–399
- [114] Wang L and Steinhardt P J, 1998 *Astrophys. J.* **508** 483–490
- [115] Smith R E, Peacock J A, Jenkins A, White S D M, Frenk C S, Pearce F R, Thomas P A, Efsthathiou G and Couchman H M P, 2003 *Mon. Not. Roy. Astron. Soc.* **341** 1311–1332
- [116] Eisenstein D J and Hu W, 1999 *Astrophys. J.* **511** 5–15
- [117] Jeong D and Komatsu E, 2006 *Preprint astro-ph/0604075*
- [118] Jain B and Bertschinger E, 1994 *Astrophys. J.* **431** 495–505